communications biology

A Nature Portfolio journal

Article

https://doi.org/10.1038/s42003-025-08449-2

TRIM33 loss reduces androgen receptor transcriptional output and H2BK120 ubiquitination

Nils Eickhoff[1,2], Janina Janetzko[1,2,7], Nuno Padrão[1,2], Sebastian Gregoricchio[1,2], Joseph C. Siefert[1,2], Liesbeth Hoekman[3], Simon Linder[1,2,8], Onno Bleijerveld[3], Andries M. Bergman[1,4,5] ✉ & Wilbert Zwart[1,2,6] ✉

The Androgen Receptor (AR) is a ligand-dependent transcription factor that drives prostate cancer development and progression. Although, a detailed effect on AR biology has been described for a number of interacting proteins, many AR coregulators remain to be characterized in relation to their distinct impact on AR function. Here, we describe TRIM33 as a conserved AR-interactor across multiple prostate cancer cell lines. We observed that TRIM33 and AR share overall chromatin interaction profiles, in which TRIM33 is involved in downstream responsive transcriptomic output. In contrast to prior reports, we show that TRIM33 does not impact AR protein stability, but instead propose a model in which TRIM33 facilitates maximal AR activity by interfering with H2BK120 ubiquitination levels.

Activation and control of transcription factor (TF) activity is essential for cellular homeostasis and adequate response to extracellular stimuli[1]. The activity of TFs can either be regulated indirectly by upstream signaling cascades (e.g., Wnt, β-Catenin[2]) or directly through ligand binding[3]. The latter group of TFs includes steroid hormone receptors, to which the estrogen, glucocorticoid and androgen receptor belong. The androgen receptor (AR) is a hormone-responsive transcription factor, that regulates the cellular response to the male sex hormone testosterone. It is well established, that the AR is involved in diseases like muscular atrophy[4], androgen insensitivity syndrome[5] and prostate cancer, in the latter being considered the key driver in development and progression of the disease[6]. This causal role in prostate cancer renders AR the main target in prostate cancer therapy[7,8]. Unfortunately, despite an initial response to AR-inhibition for most patients, eventual relapse to treatment is inevitable, as the cancer reactivates the AR signaling pathway despite low ligand levels[9]. Therefore, a more in depth mechanistic understanding of the critical components involved in AR signaling is key to improve treatment[10].

On a molecular level, AR resides in the cytosol in absence of testosterone[11]. Upon ligand binding, the receptor translocates to the nucleus, where it can bind DNA at so-called androgen receptor binding sites (ARBS), located mainly at putative enhancer elements. These are positive for enhancer-related histone marks (e.g., H3K4me1), EP300 and the active histone modification H3K27ac[12]. At these sites, AR harbors *cis*-regulatory activity to drive expression of its target genes. To facilitate alterations in gene expression, AR interacts with numerous proteins to form its canonical transcription complex and recruit the epigenetic machinery to alter DNA accessibility and local epigenetic state to finally alter transcriptional output[13].

Recent technological advances provided tools that allow for a systematic identification of AR interacting proteins in a comprehensive unbiased fashion. These technologies, such as RIME (Rapid Immunoprecipitation and Mass spectrometry of Endogenous proteins[14]), ChIP-SICAP (Chromatin Immunoprecipitation coupled with Selective Isolation of Chromatin-Associated Proteins[15]) and Bio-ID[16] identified both known and well-established AR interacting proteins as well as previously unknown AR-interacting proteins. Among these novel AR interactors are several components of the transcription intermediary factor 1 (TIF1) family[17–19], which consists of 4 proteins (TRIM24–TIF1α, TRIM28–TIF1β or KAP1, TRIM33–TIF1γ, TRIM66–TIF1δ) that belong to the tripartite motif (TRIM) containing protein family[20]. Interestingly, TRIM24, TRIM33 and TRIM66 contain nuclear receptor interacting motifs[21,22] and have all been associated with prostate cancer development[23]. What makes these proteins especially interesting in the light of transcriptional regulation is the fact that

[1]Division of Oncogenomics, The Netherlands Cancer Institute, Amsterdam, The Netherlands. [2]Oncode Institute, Utrecht, The Netherlands. [3]Mass Spectrometry/Proteomics Facility, Netherlands Cancer Institute, Amsterdam, The Netherlands. [4]Division of Medical Oncology, Netherlands Cancer Institute, Amsterdam, The Netherlands. [5]Department of Medical Oncology, Amsterdam UMC, University of Amsterdam, Amsterdam, The Netherlands. [6]Department of Biomedical Engineering, Eindhoven University of Technology, Eindhoven, The Netherlands. [7]Present address: West German Cancer Center, Molecular Oncology, Department of Medical Oncology, University Hospital Essen, Essen, Germany. [8]Present address: Division of Translational Medical Oncology, National Center for Tumor Disease (NCT) Heidelberg and German Cancer Research Center (DKFZ), Heidelberg, Germany. ✉e-mail: a.bergman@nki.nl; w.zwart@nki.nl

they contain both a Bromo and a PHD domain at their N-terminus[20]. Both domains are epigenetic readers of histone modifications allowing to potentially integrate two histone marks on one histone tail by one reader protein[24].

Here, we analyzed the AR protein interactome using RIME across six different prostate cancer cell line models and defined a core AR interactome including TRIM33. To study the role of TRIM33 in AR biology, we generated genomics and proteomics datasets of TRIM33 wildtype and knockout cell lines. We show here, that TRIM33 and AR co-occupy most of their genomic binding sites and TRIM33 loss altered expression of a subset of AR-responsive genes. In contrast to prior studies, AR levels were not affected by TRIM33 loss, and despite the canonical E3 ligase annotation of TRIM33, no indication of altered protein degradation was observed upon TRIM33 loss. Instead, we observed that TRIM33 expression coincided with reduced H2BK120 ubiquitination at genes under shared AR/TRIM33 control; a histone modification implicated in transcriptional regulation and higher order chromatin organization[25]. Altogether, we propose an alternative model of how TRIM33 impacts AR signaling, independent of protein degradation[26].

Results

TRIM33 is part of a core AR interactome across prostate cancer cell lines

To systematically characterize proteins that interact with AR across various prostate cancer disease stages, we performed AR RIME experiments in AR expressing prostate cancer cell lines that were sensitive (LNCaP, LAPC4) or resistant (CWR-R1, 22Rv1, LNCaP-abl, 42D) to hormone deprivation. An AR negative cell line (PC3) was used as a negative control. In PCA space, immunoprecipitations (Antibodies) of the IgG negative control separated clearly from the AR ones (Fig. 1A), as well as the AR positive cell lines from the AR-negative PC3 cells (Supplementary Fig. 1A). After filtering for nuclear proteins, the AR positive cell lines showed an enrichment of around 400 proteins (LNCaP = 423, LAPC4 = 304, 22Rv1 = 343, CWRR1 = 408, 42D = 433, LNCaP-abl = 385; PC3 = 35) as potential AR interactors (Supplementary Fig. 1B–H), of which 119 were shared between all (Fig. 1B and Supplementary Data 1), hereafter referred to as the "AR core interactome". Over-representation analysis of these proteins against the CORUM database of protein complexes showed enrichment for complexes involved in epigenetic regulation such as the SWI/SNF (BAF) complex, involved in nucleosome positioning, or the histone demethylase LSD1, both of which are associated with AR biology[27,28] (Fig. 1C). Interestingly, TRIM24 and TRIM33 were found in the AR core interactome and TRIM33 was also identified as a common interactor across other RIME[26] and other AR interactor studies (ChIP-SICAP[15] and AR-BioID[16], Supplementary Fig. 1I and Supplementary Data 2). TRIM24 has been extensively studied in relation to AR biology[17,29], but the impact of TRIM33 on AR is less well understood. To identify which proteins may be part of a shared TRIM33-AR complex, we next performed TRIM33 RIME in LNCaP cells with AR stimulation (5 nM R1881, 4 h) and observed enrichment of 185 nuclear proteins as potential TRIM33 interactors (Fig. 1D), of which 19 were also part of the AR core interactome (Fig. 1E). The majority of these proteins were associated with canonical AR transcriptional function including FOXA1[30], HOXB13[31], NKX3-1[32] and the SWI/SNF complex[27]. Similarly, we charted the TRIM24 interactome and we could confirm AR interaction alongside interaction with SWI/SNF members and TRIM33 (Supplementary Fig. 1J). Overall, the overlap between enriched TRIM33 and TRIM24 interactors was 49 proteins including AR, FOXA1, SWI/SNF complex members and RNF20/40.

TRIM33 and AR share chromatin binding profiles

To study if the AR/TRIM33 and AR/TRIM24 interaction is taking place on chromatin and how this may influence the epigenetic landscape, we performed ChIP-seq experiments for TRIM33 and TRIM24 and two histone marks that have been associated with the Bromo (H3K18ac) and PHD (H3K9me3) domains of TRIM33[33–35], in hormone-deprived conditions (DMSO) and two timepoints after stimulation with the synthetic androgen R1881 (4 h and 24 h) (Supplementary Fig. 2A–C).

The majority of TRIM33 peaks across all timepoints, were found in distal intergenic and intronic genomic regions, suggestive of binding to *cis*-regulatory enhancer elements (DMSO = 1695, 4 h = 1672, 24 h = 5984, averages across replicates, see Supplementary Fig. 2C), which is similar to binding patterns previously reported for AR (Fig. 2A, GSE94682[36]). Interestingly, the proportion of promoter overlapping peaks for TRIM33 was the highest in hormone-deprived DMSO conditions even though the amount of total peaks called was the lowest. In total numbers however, we observed a substantial increase of promoter-occupied TRIM33 sites upon R1881 treatment, which may be associated with increased promoter/enhancer contacts in 3D genome space. Next, we linked peaks to the closest gene and performed over representation analysis (ORA) against the cancer hallmark gene sets. The stimulated conditions showed enrichment for the androgen response pathway, suggesting that TRIM33 plays a role in the regulation of these core AR target genes (Fig. 2B). When overlapping the TRIM33 peaks with AR binding upon 4 h stimulation, most TRIM33 binding sites were shared with AR (2896; 89%), with merely 356 peaks being only present for TRIM33 (Fig. 2C). Both sets showed clear induction of TRIM33 binding upon AR stimulation, and an increase in H3K18ac signal at these sites. Interestingly, H3K18ac was also found elevated at AR peaks that did not contain TRIM33 called peaks after stimulation. This may possibly be explained by the observation that TRIM33 signal at these sites increased upon AR stimulation but not enough to pass peak calling thresholds. For H3K9me3 however, its broad distribution across repressed heterochromatin regions[37], did not allow for efficient peak calling. Nonetheless, TRIM33 peaks showed depletion of this mark at the peak center (Fig. 2C). Lastly, TRIM33 chromatin patterns were virtually completely shared with TRIM24 (Fig. 2C, D); another member of the TIF1 complex. These data indicate a possible formation of heteromeric TRIM complexes as suggested before[38,39]. Apart from peak occurrence, we also investigated the dynamic changes in TRIM33 binding upon AR activation, through identification of peaks that changed significantly in intensity between conditions. This revealed 3248 sites for TRIM33 that were gained after 4 h of stimulation compared to the hormone-deprived condition and 462 sites after 24 h that were not yet significantly increased at 4 h (Fig. 2D, E and Supplementary Fig. 2E). To see whether there are different DNA binding proteins associated with these sites, we performed motif analysis but identified mainly FOXA1 and AR motifs in both sets (Supplementary Fig. 2F). Overlapping both AR and TRIM33 called peaks at the two timepoints showed that most TRIM33 peaks are shared with AR already at 4 h of induction (Supplementary Fig. 2G). To our surprise, there was a subset of regions that showed increased TRIM33 and AR binding at 4 h but lost only the TRIM33 peak at 24 h with a slight reduction of AR signal (Supplementary Fig. 2H). Motif analysis however showed no differences in the main families of proteins associated with the distinct subsets (Supplementary Fig. 2I).

Interestingly, a distinct set of 164 TRIM33 binding sites was lost after 24 h of stimulation compared to the unstimulated control. This loss coincided with reduced H3K18ac, absence of AR binding and the spreading of H3K9me3 across the peak (Fig. 2D, E). Additionally, the TRIM24 signal already diminished upon 4 h stimulation for TRIM33 lost sites after 24 h stimulation (Fig. 2D, E). For the TRIM33 peaks located around promoters, peaks present in DMSO conditions did not show association with AR signal whereas peaks only occurring at the 24 h timepoint did show AR presence upon stimulation (Supplementary Fig. 3A). To assess which other proteins might be co-occupying these binding sites, we overlaid the TRIM33 binding site subsets with those identified in publicly available ChIP-seq data sets ($n = 13,976$) as part of the Cistrome Data Browser TF ChIP-seq sample collection[40] (Supplementary Fig. 3B). For the 4 h TRIM33 gained sites, we found enrichment of AR and its interactors (e.g., SMARCA4, FOXA1, ARID1A; Fig. 2F). Altogether, this further confirms, that TRIM33 and AR share distinct genomic binding sites and that TRIM33 recruitment to the DNA is enhanced by active AR signaling.

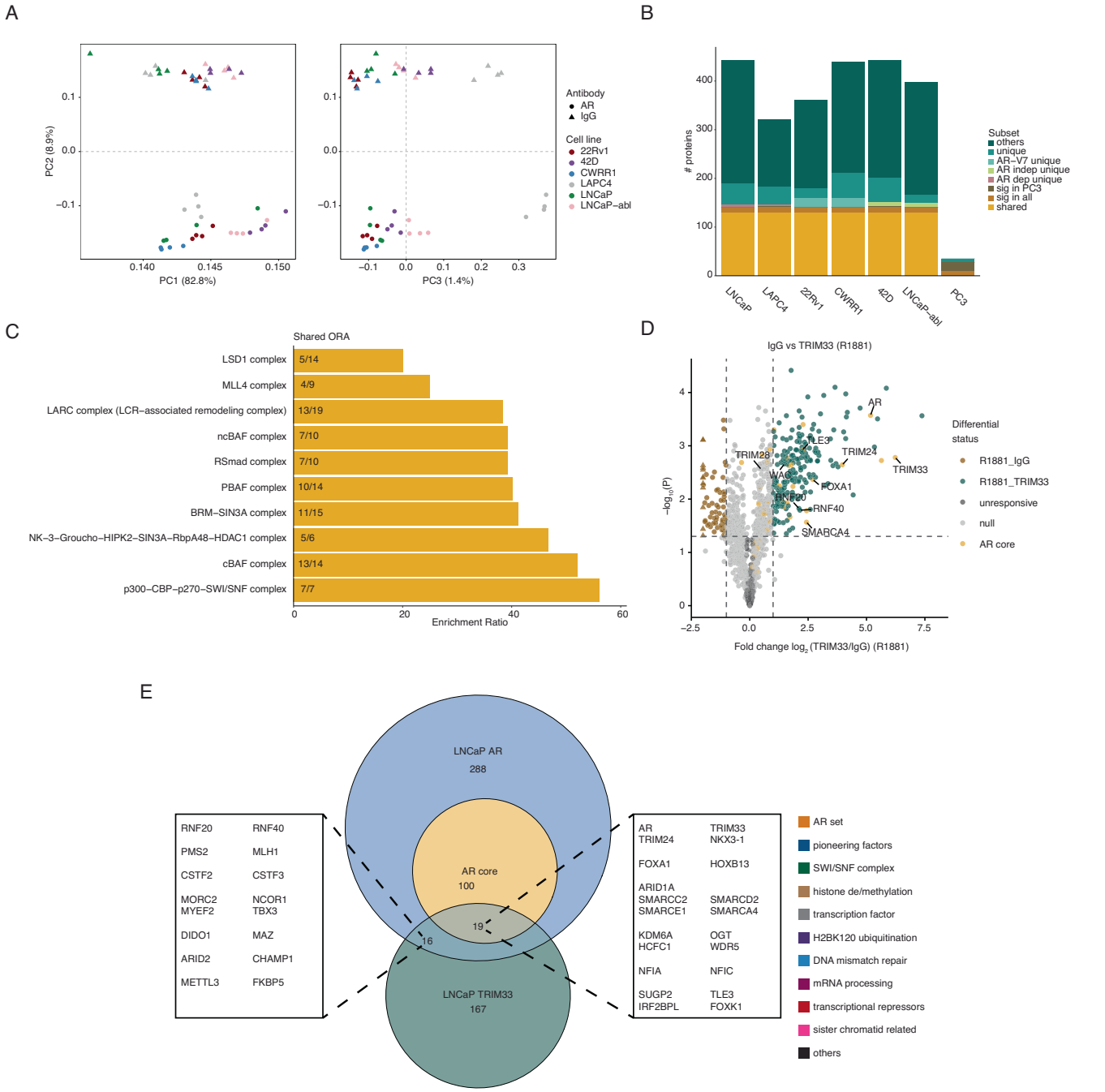

Fig. 1 | TRIM33 is part of the AR core interactome. A PCA of AR and IgG RIME data in AR positive cell lines. **B** Barplot representing the enriched nuclear proteins (LFQ difference >1 and p value < 0.05) per cell line assigned to the displayed subsets. Shared = found in all AR positive cell lines and not in PC3. Sig in all = found across all cell lines. Sig in PC3 = proteins significant in PC3 and another cell line. AR dep unique = Shared between LNCaP, LAPC4 and no other. AR indep unique = shared between CWR-R1, 22Rv1, LNCaP-abl and 42D and no other. AR-V7 unique = proteins shared in cell lines that express the alternative AR splive variant AR-V7 (CWR-R1, 22Rv1, Supplementary Fig. 3A). **C** Over representation analysis of the AR core proteins against the CORUM protein complex database. **D** Volcano plot displaying the TRIM33 RIME data with the AR core proteins highlighted in orange. Triangles depict proteins enriched in IgG with fold changes out of the axis limits. **E** Euler Diagram of the AR core, LNCaP AR and TRIM33 RIME for enriched nuclear proteins.

TRIM33 KO reduces transcription of AR target genes

To investigate the functional impact of TRIM33 on AR action, we generated CRISPR/Cas9 mediated knockouts for TRIM33 in LNCaP prostate cancer cells (Fig. 3A). In an initial analysis, we investigated whether TRIM33 influences prostate cancer cell proliferation. However, no significant or consistent differences were observed in monoclonal TRIM33-knockout lines (Fig. 3B) or polyclonal TRIM33 knockouts across LNCaP and several other prostate cancer models (Supplementary Fig. 4A–G), indicating that TRIM33 loss does not affect the proliferative potential of prostate cancer cells. Apart from its role in cancer cell proliferation, AR signaling also impacts other phenotypes, including protein secretion and cellular differentiation during development[41]. To investigate whether TRIM33 is involved in these signaling axes, we explored the transcriptomic alterations upon TRIM33 perturbations, by conducting RNA-seq experiments in two different monoclonal knockout cell lines (clones C2 and F2), the polyclonal knockout in LNCaP and 42D cells under hormone-deprived conditions and upon 6 h R1881-mediated AR activation. This short induction time reduces the potential secondary effects with the caveat of reducing the dynamic

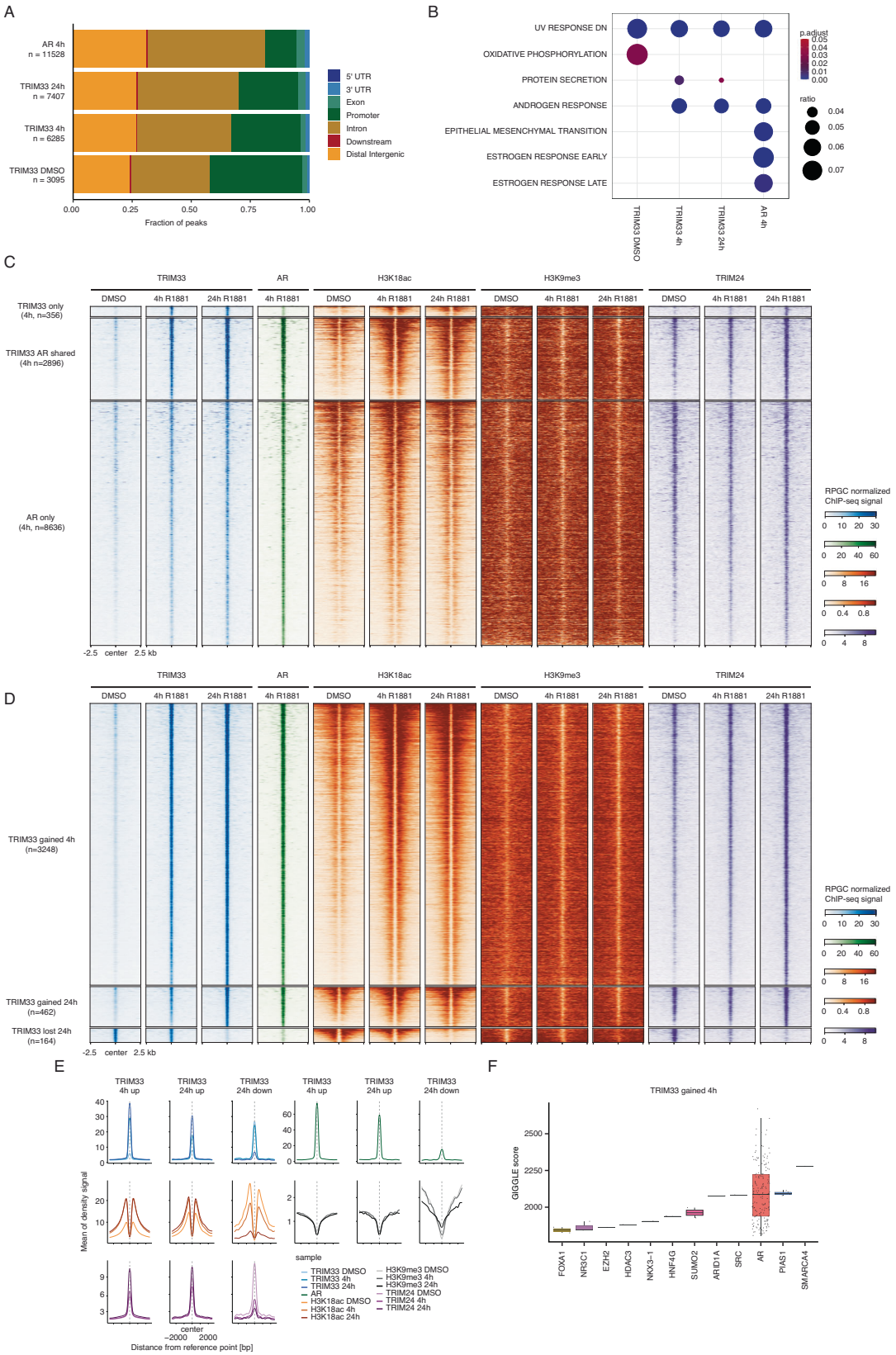

Fig. 2 | TRIM33 and AR co-occupy similar genomic locations. A Feature distribution of peaks identified in the given ChIP-seq experiment. For AR, ChIP-seq data from GSE94682 was used. **B** Over representation analysis of peak associated genes. Shown are only genesets that have a *p*.adjust <0.05. **C** Tornado plot for the TRIM33 and AR shared and unique peaks at 4 h stimulation. Data represents the average of QC passing replicates. **D** Tornado plot for the TRIM33 sites with dynamic behavior. Data represents the average of QC passing replicates. **E** Average signal intensity plots for the regions shown in (**D**). Lighter colors represent the DMSO control whereas darker colors represent stimulated conditions with R1881. **F** GIGGLE results for the TRIM33 sites gained after 4 h of R1881 treatment.

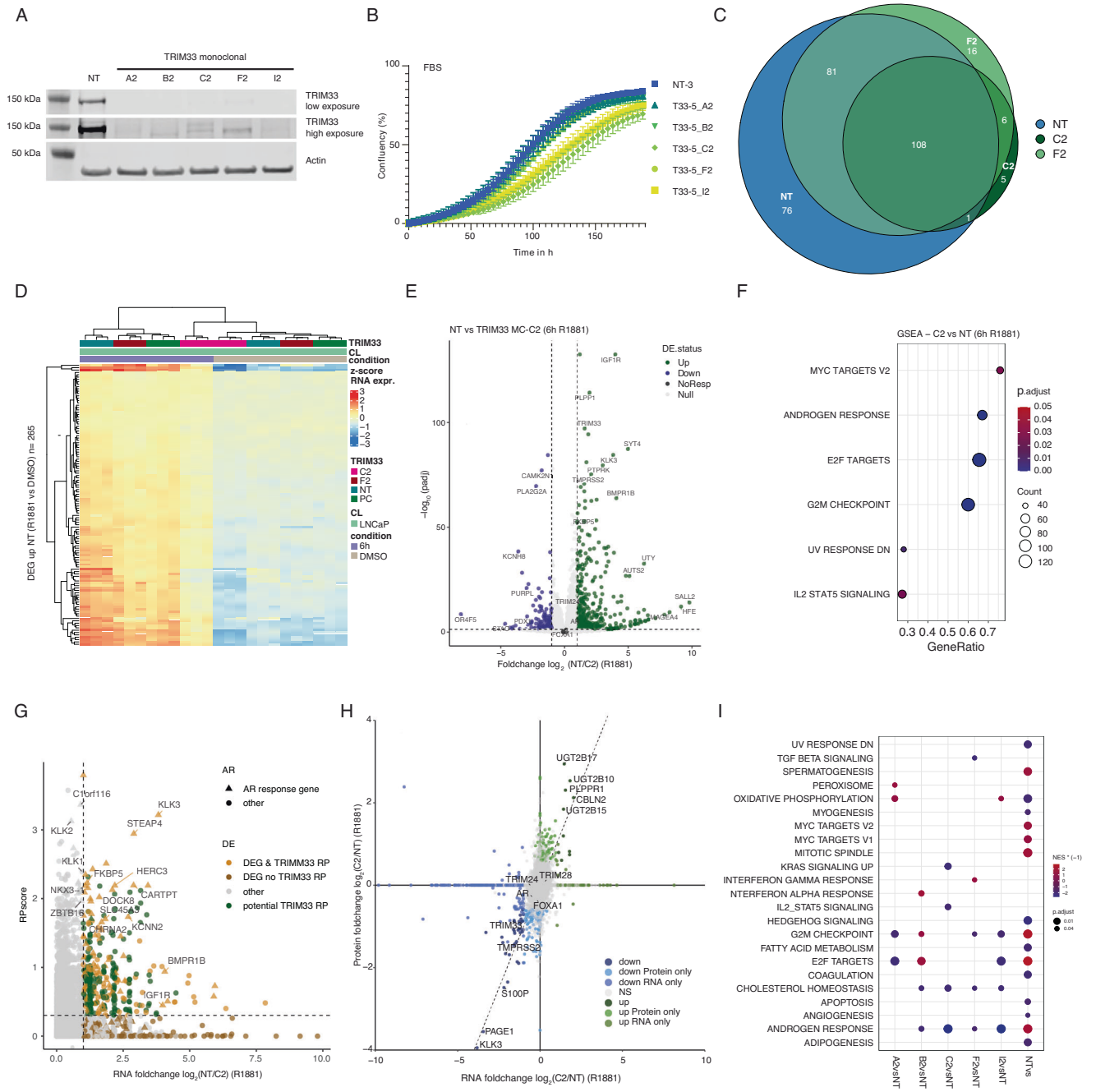

Fig. 3 | TRIM33 loss reduces AR transcriptional output. A Western blot for TRIM33 across the generated monoclonal knockout cell lines of the TRIM33-5 guide. **B** Incucyte growth curves of monoclonal TRIM33 knockout cell lines in FBS. As an error SEM is shown. **C** Euler diagram for all DEGs in the represented cell lines between DMSO and 6 h R1881 stimulation. **D** Heatmap for DEGs in the non-targeting control across all sequenced LNCaP cell lines. PC represents the TRIM33 polyclonal knockout parental cell line. **E** Volcano plot of gene expression levels between TRIM33 monoclonal knockout C2 and the non-targeting control at 6 h stimulation with R1881. Genes in green are higher expressed in non-targeting cells than knockout cells. **F** GSEA of the data in (**E**). Shown are only genesets that have a *p*.adjust <0.05. **G** Scatterplot of the Cistrome-Go analysis. Used are the TRIM33 peaks at 4 h stimulation and the RNA foldchange showed in (**E**). Triangles depict AR response genes as defined by differential expression status in non-targeting control with and without AR stimulation. Cut-off for regulatory potential was set to 0.3. **H** Scatterplot comparing TRIM33 knockout (C2) to non-targeting foldchanges on RNA (*x*-axis) and protein (*y*-axis) levels. Genes or proteins just found in one dataset were set to 0 in the other. The dashed line represents the diagonal with a slope of 1. Cut-offs for classification were a foldchange >1 for RNA and >0.5 for proteomic data. **I** GSEA of proteomic data of all tested TRIM33 knockouts in R1881 treated conditions compared to the non-targeting. NTvs represents the comparison of non-targeting cells with and without stimulation.

range. On PCA space, the two cell lines separated clearly, as well as the R1881 treated samples from the unstimulated control (Supplementary Fig. 5A). For LNCaP alone there was separation along PC1 by treatment but there was also separation along PC2 which is driven by the F2 clone (Supplementary Fig. 5B). In the non-targeting control (NT), 265 differentially expressed genes (DEGs) were detected upon 6 h R1881 treatment (Supplementary Fig. 5C). This number of treatment specific DEGs was reduced in both knockouts with 201 for F2 and 120 for C2, of which the majority overlapped with the DEGs of the control following R1881 treatment (F2: 189, C2: 108; Fig. 3C). The magnitude of decrease in AR response is in line with residual TRIM33 levels, showing the least effect in the polyclonal knockout and the most-profound effect in the monoclonal C2

knockout cell line (Fig. 3D). When comparing the stimulated conditions between control and clone C2, we observed that key AR target genes, like *KLK3*, were decreased in their expression, along with *TRIM33* itself (Fig. 3D, E). Comparable observations were made for the second clone F2 (Supplementary Fig. 6A, B). Gene set enrichment analysis (GSEA) against the cancer hallmark gene sets, showed that androgen response was downregulated in both clones, compared to the non-targeting control (Fig. 3F and Supplementary Fig. 6C, D). To investigate the potential of TRIM33 as a transcriptional regulator, we integrated the ChIP-seq and RNA-seq data streams. This analysis revealed that TRIM33 has the potential to regulate the expression of several AR responsive genes (e.g., *NKX3-1*, *FKBP5* or *STEAP4*), as well as a group of downregulated genes that do not belong to the AR signaling axis (Fig. 3G).

To further investigate AR- and TRIM33-coregulated genes, we overlapped the C2 downregulated genes in comparison to the non-targeting with the upregulated genes in the non-targeting upon AR stimulation (Supplementary Data 3). These genes associated as expected with the androgen response (Supplementary Fig. 6E) suggesting that TRIM33 is involved in a subset of general AR action, and does not drive distinct pathways under control of this transcription factor. However, some of the genes showed effects in knockout screen data across multiple cancer cell lines[42] pointing towards that some genes can play a role in proliferation when expression is abolished (Supplementary Fig. 6F). Furthermore, we observed that only a fraction of genes bound at their promoters by TRIM33 were affected by TRIM33 loss (Supplementary Fig. 6G).

As TRIM proteins, including TRIM24[43,44] and TRIM33[26,45], have been implicated as E3 ubiquitin ligases, we next explored the effect of TRIM33 loss on the proteome of LNCaP cells. Comparing these proteomics data with our transcriptomics data revealed overall a very concordant correlation between both techniques (Fig. 3H) also for the proteins that are part of the AR core (Supplementary Fig. 6H). Performing GSEA on the proteomics data showed that only androgen response and cholesterol homeostasis were downregulated in all knockouts, relative to the non-targeting control (Fig. 3I). Jointly, these data suggest that the observed effects are mainly driven by transcriptional changes due to TRIM33 loss rather than post-translational protein degradation. Additionally, we do not observe changes of AR protein levels, which is in contrast to prior work that linked TRIM33 and AR degradation via SKP2[26] (Supplementary Fig. 6I).

Lastly, we analyzed whether TRIM33 absence would affect the AR interactome, but no differences in the AR interactome were observed between KO and non-targeting controls, except for TRIM33 itself (Supplementary Fig. 6J).

TRIM33 loss reduces H2BK120ub at AR target genes

As TRIM33 is the reader of H3K18ac, we next checked if loss of TRIM33 affected H3K18ac stability or AR binding to the chromatin. Therefore, we performed ChIP-seq for AR and H3K18ac in the TRIM33 knockout and non-targeting cell lines (Fig. 4). Additionally, we took along H2BK120 ubiquitination (H2Bub), a marker for active transcription across gene bodies[25], as it has been reported that TRIM33 and TRIM24 work in concert to facilitate this mark at the *HSP72* promoter together with HSF1 in HeLa cells[38]. In PCA space, the different IP targets (AR, H3K18ac, H2Bub) formed distinct clusters (Fig. 4A top left). Individual analysis for each target showed no clear separation between knockout and control samples. Instead, the primary distinction was between untreated and R1881-stimulated samples (Fig. 4A). For H2Bub the least differences could be observed in PCA space, which could be explained by the fact that the majority of gene bodies throughout the genome are not affected by TRIM33 loss and a more focused approach is needed (Fig. 4A and Supplementary Fig. 7A, B). Differential binding analysis between TRIM33-KO and control across all timepoints showed no differences for H2Bub and a small fraction of peaks changing for both H3K18ac and AR (Supplementary Fig. 7C, D). Density profiles at the small subset of TRIM33-KO affected peaks for AR and H3K18ac showed weak binding and noisy behavior, suggesting that these might be artifacts (Supplementary Fig. 7C, D, top panels). Across the identified differential binding sites for TRIM33 after stimulation, the signal intensities were relatively similar across all subsets (Fig. 4B). We then tested whether TRIM33-KO affected H2Bub signal for genes that are differentially expressed upon TRIM33 perturbation, as determined by RNA-seq (Fig. 3D). Upregulated genes in TRIM33-KO cells had higher levels of H2Bub compared to non-targeting control (Fig. 4C, D). Interestingly, AR stimulation reduced H2Bub at these sites in both the knockout as well as the non-targeting compared to the unstimulated condition. For the genes downregulated upon TRIM33 knockout, the opposite behavior was observed, with higher H2Bub in the non-targeting as compared to the knockout cell line. Statistical analyses (with a p-value cut-off of 0.01) showed that only the differentially expressed genes are affected on H2Bub levels whereas the H2Bub signal for unresponsive genes was not altered (Fig. 4E).

Together these data support the notion that TRIM33 is neither affecting AR chromatin occupancy nor AR turnover, but instead impacts the transcriptional output of AR target genes (Supplementary Fig. 8A–C). In this role, TRIM33 is required for full AR activity, which is tightly associated with distinct alterations in H2BK120 ubiquitination in a locus-specific manner.

One reason for limited effect of TRIM33 on AR biology could be that TRIM24 compensates for TRIM33 loss. Using a TRIM24 PROTAC[46,47] we efficiently depleted TRIM24 protein levels upon 48 h treatment in LNCaP cells (Supplementary Fig. 8D). In the TRIM33 knockout cells, PSA levels were not further reduced upon TRIM24 PROTAC exposure, and total levels of H3K18ac and H3K23ac (TRIM24 read histone mark[48]) did not change (Supplementary Fig. 8E).

Finally, we investigated the role of TRIM33 in a non-transformed cell line, as well as in clinical specimens[49]. After neoadjuvant treatment with AR inhibitors (Enzalutamide) for 3 months, TRIM33 expression was reduced in human prostate tumors (Supplementary Fig. 8F). On the other hand, in the normal like prostate cancer cell line LHS-AR[31,50], knockdown of TRIM33 with siRNA reduced several AR and TRIM33 target genes identified in LNCaP cells (Supplementary Fig. 8G). Cumulatively, these analyses show that TRIM33 serves as a bona fide AR coregulator, both in the oncogenic setting as well as in non-malignant conditions.

Discussion

Despite advances in better understanding the AR cistrome throughout the development, treatment and progression of prostate cancer[31,49,51], the effect of non-DNA binding cofactors on AR biology remains incompletely understood. Furthermore, while it is established that distinct AR-subcomplexes form on a genome-wide scale[36], the implications thereof remain understudied. Here we characterized TRIM33 in the light of AR biology, and showed that TRIM33 is required for complete transcriptional output of AR at distinct genomic locations. While TRIM33 loss decreased activity of the canonical AR responsive geneset, proliferation of AR-driven prostate cancer cells was not affected by TRIM33 knockout. As the AR serves numerous roles beyond proliferation alone[52–55], these findings suggest that deviations in the AR transcription complex composition over different AR-responsive genes, as we reported previously[36], may give rise to distinct dependencies of subsets of AR-driven genes to specific coregulators; such as TRIM33.

The observed changes are associated with alterations in H2BK120 ubiquitination status at TRIM33/AR-coregulated genes. This finding is in contrast to the previously reported role of TRIM33 on AR biology, that reported TRIM33 levels to affect AR protein levels via SKP2[26]. These discrepancies could be due to the different depletion methodologies and timeframes, as the authors of the prior report used transient siRNAs for depletion, while the current study made use of stable CRISPR/Cas9 mediated knockout models. To investigate whether these discrepancies were due to the different methodologies in TRIM33 depletion, we carried out experiments employing both the TRIM33 siRNAs described in the prior study[26] as well as the commercially available siRNA SMARTpool (Dharmacon). Surprisingly, while in our hands only the SMARTpool showed on-target depletion of TRIM33, none of the siRNAs had any effect on AR

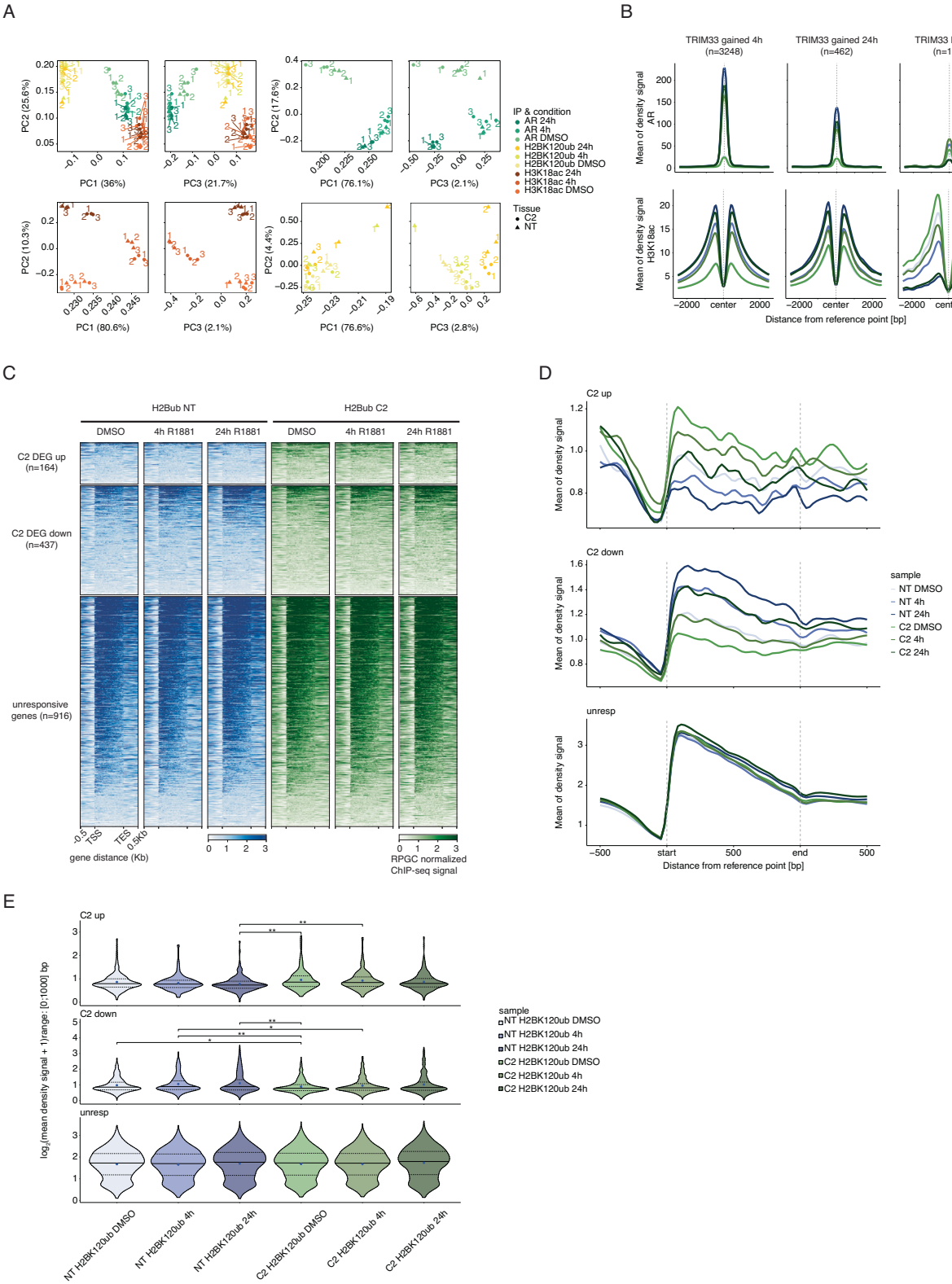

Fig. 4 | AR target genes have lower H2Bub levels in TRIM33 knockout cells. **A** PCA plots for grouped and individual analysis of the TRIM33 C2 knockout ChIP-seq data. **B** Average signal intensity profiles of AR (top) and H3K18ac (bottom) across the tested cell lines on the TRIM33 R1881 treatment gained and lost regions of Fig. 2D. TRIM33 C2 knockout cells are in green and non-targeting in blue. **C** Heatmap of H2Bub signal across gene bodies of differentially expressed genes from Fig. 3E as well as the unresponsive genes. **D** Average signal intensity plots for the regions depicted in (**C**). **E** Distribution of the sum of the H2Bub signals across the scaled gene body from the regions in (**C**). Significance levels of Wilcoxon ranked sum test: * < 0.01, ** < 0.001.

protein levels (Supplementary Fig. 9). Further investigations would be needed to resolve these inconsistencies between the two studies.

TRIM24, TRIM28 and TRIM33 are all members of the TIF1 complex, and while prior studies have investigated the relative contributions of TRIM24 and TRIM28 on AR biology, TRIM33 remains largely understudied. While TRIM33 is classically annotated as a E3 ligase, our data suggest that TRIM33 mostly acts on the transcriptional level, rather than altering the proteome through post-translational ubiquitination. It is important to consider that not all ubiquitin modifications lead to proteasomal degradation of the ubiquitinated protein[56]. Therefore it is possible that TRIM33 is involved in other ubiquitin linkages, like it has been shown for TRIM24[44] or mono-ubiquitination as is suggested for H2BK120. For the latter, even though recruited individually, prior work reported that H2Bub was only deposited when both TRIM24 and TRIM33 were present[38]. Our study cannot clearly decipher whether TRIM33 is actively influencing H2Bub or whether the altered H2B ubiquitination is a consequence of reduced transcription through TRIM33 action on AR enhancers. It is also possible that TRIM33 ubiquitinates other proteins in the AR complex, altering their action in a proteasome independent fashion. Implementation of ubiquitin-specific probes may shed light on these possibilities.

Notably, TRIM33 plays a role in transcription regulation at merely a subset of AR sites. These observations highlight that cofactors are not universal at all AR binding sites, leading to subcomplexes owing distinct functions (Stelloo et al.[36]). In our study, while we observed that proliferation is not affected by TRIM33 knockout, hallmark AR target genes are nonetheless downregulated. These data implicate that the hallmark AR gene set does not reflect the role of AR in proliferation, but rather is indicative for its role in other cellular functions. To better capture the oncogenic roles of AR, it may prove critical to rather select genes affected in clinical transitions in tumorigenesis or metastasis formation instead[57].

Current technologies for AR protein interactomes are averaged across all binding sites, which leads to a loss of dependencies and co-occurrences between proteins in the AR complex. Single locus transcription factor complex analyses have been shown to be possible, but remain technically highly challenging[58]. Alternatively, overlaps of interactomes of several AR interactors can shed light on co-occurrence patterns, as we can see here for the 35 proteins shared between AR and TRIM33 in LNCaP cells. In general, the interactome datasets between orthogonal measures appears surprisingly small, highlighting the necessity of stringent controls and analysis to increase true positive hits.

Altogether, we confirm the action of TRIM33 as a coactivator of AR, however not via AR stability but rather through attenuating maximal transcriptional activity potentially by altering H2Bub levels in a locus-specific manner. Even though not impacting prostate cancer cell proliferation in our hands, TRIM33 appears crucial for the expression of canonical AR target genes. Our results provide a deeper mechanistic understanding of transcriptional regulation by AR in prostate cancer, that may serve as a fundamental basis for translation of these concepts towards the oncological setting.

Methods

Cell culture

LNCaP, 22Rv1, CWRR1, PC3, LAPC4 and HEK293T were purchased from ATCC, LNCaP-abl, 42D were a generous gift from Amina Zoubeidi (Vancouver) and LHS-AR cells were a generous gift from M. Freedman (Boston). Prostate cancer cell lines were cultured in RPMI 1640 medium (Gibco, Thermo Fisher Scientific) supplemented with Penicillin/Streptomycin (Gibco, Thermo Fisher Scientific; 1U, 1 µg/ml) and 10% FBS (LNCaP, 22Rv1, CWR-R1, LAPC4; Capricorn) or 5% of dextran and charcoal stripped FBS (DCC, LNCaP-abl). 42D cells were continuously cultured in the presence of 10 µM Enzalutamide (MedChemExpress). HEK293T cells were cultured in DMEM medium (Gibco, Thermo Fisher Scientific) supplemented with Penicillin Streptomycin and 10%FBS. For experiments involving hormone stimulation, cells were cultured in DCC for 72 h prior to the start of the experiment. Cells were regularly tested for *Mycoplasma* and were authenticated by short tandem profiling (Eurofins Genomics).

Knockout generation

Guides targeting TRIM33 (T33-3: 5'-ACAGAGTCTGTTGGAGCATC-3, T33-4: 5'-ACTATGGCAAATGCAAACCG-3, T33-5: 5'-CTCCTCCTCCACCAGCACCG-3) or non-targeting control (NT: 5'-AACTACAAGTAAAAGTATCG-3) were cloned into lentiCRISPRv2 plasmids (ref. 59 Addgene: #52961). For lentivirus production, CRISPR plasmids were cotransfected with 3rd generation lentiviral plasmids (5:1:1:1) using polyethylenimine (Polysciences) into HEK293T cells. Virus containing supernatants were harvested, filtered using a 0.22 µm anti-pyrogenic filter, and stored at −80 °C until use. Two days post transduction, cells were selected with puromycin (Sigma-Aldrich, 2 µg/ml) for 2 weeks and knockout efficiencies were estimated using western blotting. For monoclonal cell lines, polyclonal parental cells were FACS sorted into 96 well plates (Greiner, Cellstar) and gradually grown out.

Western blot

Whole cell lysates were prepared using a 2x Laemmli lysis buffer supplemented with EDTA-free complete protease inhibitor cocktail (Roche), 100 mM NaF (Thermo Scientific) and 2 mM Na_3VO_4 (Jena Bioscience). Lysates were sonicated for 10 cycles 1 s on/off with a probe sonicator (Active Motif) at 20% amplitude. Protein amounts were measured using the Pierce BCA protein assay kit (Thermo Fisher Scientific) according to the manufacturer's instructions. Then 30 µg of protein were reduced using 0.1 M DTT (Sigma Aldrich) and loaded onto 4–12% Bis-Tris NuPAGE gels, run in MOPS buffer and subsequently wet transferred onto 0.45 µm nitrocellulose membranes (Santa Cruz Biotechnology). Membranes were blocked in 5% fat-free milk in PBS-0.001% Tween20 (Sigma Aldrich) prior to overnight incubation at 4 °C with primary antibodies (Actin: MAB1501R, Merck, 1:3500; TRIM33: D7U4F, Cell Signaling Technologies, 1:1000, 1:1000; AR: 06-680, Merck, 1:1000; H3K18ac: C15410139, Diagenode, 1:1000; H3K23ac: 39131, Active Motif, 1:2500; TRIM24: 100-2596, Novus Biological, 1:1000; PSA: 5365S, Cell Signalling, 1:1000). Subsequently, the membranes were incubated with appropriate IRDye® secondary antibodies (680 or 800 nm, LI-COR, 1:10,000). Signal detection was carried out using an Odyssey CLx imager (LI-COR) and image analysis was performed using Image Studio Lite (v5.5)

Cell proliferation

Incucyte. A total of 1000 LNCaP cells were seeded in 384-well plates in DMSO or 10 µM Enzalutamide (MedChemExpress) containing medium. After 24 h the plate was transferred into an Incucyte® ZOOM live cell analysis system (Sartorius) and wells were imaged every 4 h over the course of the experiment. Confluency was calculated with the build-in software with an adjusted mask (Segmentation adjustment = 0.1, Hole fill ≤40 µm^2, Area ≥500 µm^2).

CellTiter-Glo. CellTiter-Glo (Promega) assays were used as an orthogonal method to measure cell viability. Cells were seeded into 384-well plates (LNCaP: 750, LAPC4: 1000, 42D: 1000, CWRR1: 500; all cells/well). After 24 h cells were treated either with DMSO or 10 µM Enzalutamide and, after 7 days, signal was measured according to the manufacturers protocol and analyzed using GraphPad Prism (9.4.1).

Whole cell proteomics

For whole cell proteomics, 700,000 LNCaP cells were seeded in a 6cm-dish. 48 h later the cells were washed twice with cold PBS on ice and then scraped twice in 500 µL PBS. Cells were pelleted at 1000 rpm at 4 °C for 5 min. The supernatant was removed and the pellets frozen in liquid nitrogen, and stored at −80 °C until further processing.

For protein digestion, frozen tissues were lysed in boiling Guanidine (GuHCl) lysis buffer as described before[60]. Protein concentration was determined with a Pierce Coomassie (Bradford) Protein Assay Kit

(Thermo Scientific), according to the manufacturer's instructions. After dilution to 2 M GuHCl, aliquots corresponding to at least 1.05 mg of protein were digested twice (4 h and overnight) with trypsin (Sigma-Aldrich) at 37 °C, enzyme/substrate ratio 1:75. Digestion was quenched by the addition of FA (final concentration 5%), after which the peptides were desalted on a Sep-Pak C18 cartridge (Waters, Massachusetts, USA). From the eluates, aliquots were collected for proteome analysis and samples were vacuum dried and stored at −80 °C until LC-MS/MS analysis.

Prior to mass spectrometry analysis, the peptides were reconstituted in 2% formic acid. Peptide mixtures were analyzed by nanoLC-MS/MS on an Orbitrap Exploris 480 Mass Spectrometer equipped with an EASY-NLC 1200 system (Thermo Scientific). Samples were directly loaded onto the analytical column (ReproSil-Pur 120 C18-AQ, 2.4 µm, 75 µm × 500 mm, packed in-house). Solvent A was 0.1% formic acid/water and solvent B was 0.1% formic acid/80% acetonitrile. Samples were eluted from the analytical column at a constant flow of 250 nl/min. For single-run proteome a 90-min gradient was employed containing a 78-min linear increase from 6 to 30% solvent B, followed by a 12-min wash.

Raw data were analyzed by DIA-NN (version 1.8)[61] without a spectral library and with "Deep learning" option enabled. The Swissprot Human database (20,395 entries, release 2022_02) was added for the library-free search. The Quantification strategy was set to Robust LC (high accuracy) and MBR option was enabled. The other settings were kept at the default values. The protein groups report from DIA-NN was used for downstream analysis in Perseus (version: 1.6.15.0)[62]. Values were Log2-transformed, after which proteins were filtered for at least 2 out of 3 valid values in at least one sample group.

RIME experiments

Six confluent 15 cm-dishes of a cell line cultured in DCC for 72 h were induced with 5 nM R1881 or DMSO for 4 h before fixing with 1% formaldehyde (Electron Microscopy Sciences) for 10 min. Samples were processed as described in Mohammed et al. In brief, cells were harvested and chromatin was sonicated with a Bioruptor pico (Diagenode) sonicator using cycles of 30 s on/off until obtaining a fragment sizes around between 250–700 bp. 10 µg of AR, TRIM24 or TRIM33 antibody were coupled to 50 µL protein A dynabeads (Invitrogen, cat. 10008D) for immunoprecipitation. After over-night immunoprecipitation, beads were washed with RIPA-RIME buffer and 100 mM ammonium bicarbonate and stored at −80 °C until on bead tryptic digest was performed and protein content quantified.

Mass spectrometry. For mass spectrometry, peptide mixtures were prepared and measured as previously described (Stelloo et al. [36]), with the modifications described below.

Peptide mixtures (10% of total digest) were loaded directly onto the analytical column and analyzed by nLC-MS/MS using a mass spectrometer connected to a nLC system as described in Supplementary Table 1. Solvent A was 0.1% formic acid/water and solvent B was 0.1% formic acid/80% acetonitrile. Peptides were eluted from the analytical column at a constant flow of 250 nL/min in a linear gradient, see Supplementary Table 1 for gradient details. Raw data were analyzed by MaxQuant (see Supplementary Table 2, MaxQuant version)[63] using standard settings for label-free quantitation (LFQ). MS/MS data were searched against the Human database (see Supplementary Table 2, database) complemented with a list of common contaminants and concatenated with the reversed version of all sequences. The maximum allowed mass tolerance was 4.5ppm in the main search and 0.5 Da for fragment ion masses. False discovery rates for peptide and protein identification were set to 1%. Trypsin/P was chosen as cleavage specificity allowing two missed cleavages. Carbamidomethylation (C) was set as a fixed modification, while oxidation (M) and deamidation (N, Q) were used as variable modifications. LFQ intensities were Log2-transformed in Perseus (see Supplementary Table 2)[62], after which proteins were filtered as described in Supplementary Table 2.

LFQ data was then further processed using *DEprot* (https://github.com/sebastian-gregoricchio/DEprot), using the built-in missForest algorithm[64] to impute missing data. Differential protein abundance was defined as p value < 0.05 (paired t-test) and |LFQ difference | > 1. For RIME experiments, over-representation analysis using the WebGestalt[65] webtool was used against the CORUM database (v5) at default parameters for enriched proteins using the protein coding genome as a background. For whole cell proteomics the LFQ difference was used as a ranking metric before using clusterProfiler for GSEA.

ChIP-seq experiments

For ChIP-seq experiments 42×10^6 LNCaP cells were seeded per condition in DCC containing medium. After 72 h cells were treated with 5 nM R1881 or DMSO for 4 h or 24 h. Cells were fixed in 1% formaldehyde (Sigma-Aldrich) for 10 min and quenched with 0.125M L-glycine (Sigma-Aldrich). Cells were scraped on ice in PBS containing cOmplete EDTA-free protease inhibitor cocktail (Roche), pelleted at 2000 rcf for 5 min at 4 °C and stored at −80 °C until further processing. ChIP-seq and QC was performed as previously described[66,67] with the following modifications: Cell pellets were thawed on ice, resuspended in lysis buffer 1 (LB1: 50 mM Hepes, 140 mM NaCl, 1 mM EDTA, 10% glycerol, 0.5% NP40, 0.25% Triton-X100, KOH to pH 7.5; 10×10^6 cells/mL) and incubated on a rotator for 10 min at 4 °C. Nuclei were pelleted at 2000 rcf for 5 min at 4 °C. Pellets were resuspended in lysis buffer 2 (LB2: 10 mM Tris, 200 mM NaCl, 1 mM EDTA, 0.5 mM EGTA, HCl to pH 8; 10×10^6 cells/mL), incubated on a rotator for 10 min at 4 °C and centrifuged at 2000 rcf for 5 min at 4 °C. Washed nuclei were resuspended in lysis buffer 3 (LB3: 10 mM Tris, 100 mM NaCl, 1 mM EDTA, 0.5 mM EGTA, 0.1% Na-DOC, 0.5% lauroylsarcosine, HCl to pH 8; 30×10^6 cells/mL). Nuclei were sonicated for 14 cycles (30 s on/off) using a PicoBioruptor (Diagenode) and chromatin was checked to be at a size around 250 bp using agarose gel electrophoresis. Triton-X100 was added to the sheared chromatin at a final concentration of 1% and debris were pelleted for 12 min at 20,000 rcf at 4 °C. The supernatant was then incubated overnight under rotation at 4 °C with 50 µL (1.5 mg) of Protein A Dynabeads (Invitrogen), previously incubated with 5 µg of the respective antibody (AR, TRIM33: as above, TRIM24: NB100-2596, Novus Biologicals, H3K18ac: C15410139, Diagenode, H3K9me3: ab8898, Abcam). Beads were then washed 10 times with RIPA-ChIP buffer (50 mM HEPES, 500 mM LiCl, 1 mM EDTA, 1% NP-40, 0.7% Na-DOC, pH = 7.6), washed once in TBS and reverse cross-linked at 65 °C in 200 µL of Elution Buffer (EB: SDS 1%, 50 mM Tris, 10 mM EDTA) for 12–16 h. Upon 30 min treatment with 40 µg RNase A (Life Technologies), 1 h treatment with PK buffer (10 µL 0.5 M EDTA, 20 µL 1 M Tris-HCl pH 6.5, 40 µg Proteinase K (Invitrogen)), ChIP DNA was purified using phenol/chloroform/isoamylalcohol (25:24:1, pH 8.0, Thermo Scientific) and precipitated with 2 volumes of 100% ethanol. Illumina multiplex-sequencing with 51 bp paired-end setup was performed on the NovaSeq 6000 (Illumina) sequencer following manufacture instructions. All ChIP-seq samples were processed using the *SPACCa* pipeline (available at https://github.com/sebastian-gregoricchio/SPACCa) using default parameters. Briefly, FASTQ reads were mapped to the reference genome Hg38/GRCh38 using the accelerated version of the Burrows-Wheeler Aligner (BWA-MEM2 v0.5.10[68]. Reads were filtered based on mapping quality (MAPQ ≥ 20), and duplicated reads were removed and RPGC normalized. Samples that did not pass QC were removed and all samples had at least 2 biological replicates (TRIM33 4 h, TRIM33 24 h).

Differential peak analyses were performed using DiffBind[69] using the DESeq2 mode and applying a threshold of 1 for the $|\log_2(\text{fold-change})|$ and 0.05 for the false discovery rate (FDR). Signal of three biological replicates was averaged per condition using the *bigwigAverage* function from deepTools[70].

Annotation of peaks to genomic regions and overrepresentation analysis was done with ChIPseeker[71] and clusterProfiler[72] respectively with default parameters (TSS region = ±3 kb). Tornado plots were generated with the *computeMatrix* and *plotHeatmap* functions from deepTools. Density plots were generated using the *plot.density.profile* function from

Table 1 | Primers used in qPCR experiments for the indicated target

Target	Forward	Reverse
TBP	GTTCTGGGAAAATGGTGTGC	GCTGGAAAACCCAACTTCTG
TRIM33	ACAGCGGCCCTCAATATTCC	GCTGTAACAGATGGGCTGGT
TMPRSS2	TCACTAGGTCGTTGAAAGTCAGA	TGGAGCCGGATACCAAGTAGA
FKBP5	AATCAAGGAGCTCAATCTCAAAAA	TATGCATATGGCTCGGCTGG
GRHL2	CGCCTATCTCAAAGACGACCAG	CCAGGGTGTACTGAAATGTGCC
ZBTB16	GAGCTTCCTGATAACGAGGCTG	AGCCGCAAACTATCCAGGAACC
SALL2	TGGCACTGAGTGCTGTTGTGGA	GGCTTGCCTTATGGTATGTCCG
MSI1	GCGTAGGTTGTGGCTTGGAAAC	GCGTAGGTTGTGGCTTGGAAAC

Rseb (ref. 73, https://github.com/sebastian-gregoricchio/Rseb). For these, the bigwig files of QC passing replicates were merged using *bigwigAverage* from deeptools with a bin size of 50 bp. These files were also used for pyGenomeTracks from deeptools to make the tracks of a genomic region of interest. The obtained images were then adjusted in Adobe Illustrator.

GIGGLE analysis was performed using the CistromeDB toolkit (http://dbtoolkit.cistrome.org) with top 10k peaks and default parameters and the data was replotted in R.

Motif analysis was performed for the given bed files using the MEME suite[74] AME[75] tool for the HOCOMOCO v12[76] dataset with default conditions. Wordclouds were replotted using ggwordcloud in R.

RNA-seq

For RNA-sequencing, cells were seeded with a density of 1×10^6 cells (LNCaP) and 7.5×10^5 (42D) cells in a 6cm-dish in DCC. After 72 h of hormone deprivation, cells were either treated with 10 nM R1881 or DMSO for 6 h. RNA was isolated using the RNeasy column purification and DNAse kit (Qiagen) according to the manufacturer's instructions. Libraries were prepared using the Illumina TruSeq polyA stranded RNA prep kit and subsequently sequenced on the NovaSeq 6000 platform. Paired-end 51 bp reads were deduplicated and quality checked before aligning to hg38 using TopHat2[77]. Count matrices were filtered for genes with at least 1 valid count and then used for Differential expression analysis using DEseq2[78] with thresholds of adjusted p value < 0.05 and $|\log_2(\text{fold-change})| > 1$. GSEA was performed using clusterProfiler. Heatmaps were generated using the pheatmap R package[79] and data was previously vst normalized.

Linking of ChIP-seq and RNA-seq data was performed using Cistrome-GO[80] with default parameters. Regulatory potential thresholds were RP score >0.3 and $\log_2$(fold-change) >1.

siRNA knockdown

siRNAs targeting TRIM33 (siT33-1: 5'-GUCAGUUUUCUGAUAGAC-3' | 5'-AAUAGUGGUCUAUCAGAA-3', siT33-2: 5'-GGUGAAGCAUG UUAUGA-3' | 5'-UGUGAAGUUCAUAACAUG-3') from a previously published paper[26] were ordered as duplexed RNA molecules from IDT as they were too short to be ordered as DsiRNAs but the non-targeting could be ordered as a DsiRNA (siNT-I: 5'-GAACCAGCCAAGGUAGACAGUC AGA-3' | 5'-UCUGACUGUCUACCUUGGCUGGUUCCU-3'). Additionally, a Dharmacon non-targeting (siRNA pool #5) and an ON-TARGETplus TRIM33 siRNA SMARTpool was ordered.

300,000 LNCaP or 200,000 LHS-AR cells were seeded in a 6-well plate in phenol red free RPMI medium. 24 h after seeding, the cells were transfected according to the RNAiMAX (Thermo Scientific) protocol and 48 h later protein or RNA was harvested.

TRIM24 PROTAC experiments

dTRIM24 (Medchemexpress, HY-111519) was dissolved in DMSO and used in the indicated concentrations. Cells were seeded as described above for western blot experiments and treated 24 h after seeding.

qPCR

siRNA treated cells were washed with PBS before being harvested with TRIzol (Thermo Scientific) reagent. RNA was purified according to the manufacturers protocol. Subsequently 2 µg of RNA were used as input in reverse transcription using the SuperScript-II kit (Thermo Scientific) with random hexamer primers. The obtained cDNA was diluted 1:100 and 1.5 µl per sample and reaction were used in the SensiMix no-Rox kit (Meridian Bioscience). Three technical replicates were run per primer and sample. Primers were used at 300pM and sequences can be found in Table 1.

Euler graphs

Euler graphs were calculated using the eulerr web tool (https://eulerr.co) and adjusted in Adobe Illustrator. Larsson J (2021). *eulerr: Area-Proportional Euler and Venn Diagrams with Ellipses*. R package version 6.1.1, https://CRAN.R-project.org/package=eulerr.

Statistics and reproducibility

All experiments have been performed in three independent biological replicates. Where applicable, technical replicates were included (qPCR = 3, Incucyte = 5, CTG = 5). When statistical significance levels are depicted in the figures, the used test can be found in the figure legend.

Reporting summary

Further information on research design is available in the Nature Portfolio Reporting Summary linked to this article.

Data availability

Mass spectrometry data have been deposited at the ProteomeXchange Consortium through the PRIDE[81] partner repository with the identifier PXD058914. All sequencing data generated in this study (RNA-seq and ChIP-seq) have been deposited on GEO under accession number GSE284522. Uncropped images of all western blots displayed can be found in Supplementary Fig. 10.

Received: 14 January 2025; Accepted: 26 June 2025;
Published online: 11 July 2025

References

1. Spitz, F. & Furlong, E. E. M. Transcription factors: from enhancer binding to developmental control. *Nat. Rev. Genet.* **13**, 613–626 (2012).
2. Liu, J. et al. Wnt/β-catenin signalling: function, biological mechanisms, and therapeutic opportunities. *Sig. Transduct. Target Ther.* **7**, 3 (2022).
3. Weikum, E. R., Liu, X. & Ortlund, E. A. The nuclear receptor superfamily: a structural perspective. *Protein Sci.* **27**, 1876–1892 (2018).
4. Spada, A. R. L., Wilson, E. M., Lubahn, D. B., Harding, A. E. & Fischbeck, K. H. Androgen receptor gene mutations in X-linked spinal and bulbar muscular atrophy. *Nature* **352**, 77–79 (1991).

5. McPhaul, M. J., Marcelli, M., Tilley, W. D., Griffin, J. E. & Wilson, J. D. Androgen resistance caused by mutations in the androgen receptor gene. *FASEB J.* **5**, 2910–2915 (1991).
6. Lonergan, P. E. & Tindall, D. J. Androgen receptor signaling in prostate cancer development and progression. *J. Carcinog.* **10**, 20 (2011).
7. Eickhoff, N., Bergman, A. M. & Zwart, W. Homing in on a moving target: androgen receptor cistromic plasticity in prostate cancer. *Endocrinology* **163**, bqac153 (2022).
8. Huggins, C. Prostatic cancer treated by orchiectomy; the five year results. *J. Am. Med. Assoc.* **131**, 576–581 (1946).
9. Waltering, K. K. et al. Increased expression of androgen receptor sensitizes prostate cancer cells to low levels of androgens. *Cancer Res.* **69**, 8141–8149 (2009).
10. Jafari, H., Hussain, S. & Campbell, M. J. Nuclear receptor coregulators in hormone-dependent cancers. *Cancers* **14**, 2402 (2022).
11. Jenster, G., Trapman, J. & Brinkmann, A. O. Nuclear import of the human androgen receptor. *Biochem. J.* **293**, 761–768 (1993).
12. Gasperini, M., Tome, J. M. & Shendure, J. Towards a comprehensive catalogue of validated and target-linked human enhancers. *Nat. Rev. Genet.* **21**, 292–310 (2020).
13. Altıntaş, U. B. et al. Decoding the epigenetics and chromatin loop dynamics of androgen receptor-mediated transcription. *Nat. Commun.* **15**, 9494 (2024).
14. Mohammed, H. et al. Rapid immunoprecipitation mass spectrometry of endogenous proteins (RIME) for analysis of chromatin complexes. *Nat. Protoc.* **11**, 316–326 (2016).
15. Launonen, K.-M. et al. Chromatin-directed proteomics-identified network of endogenous androgen receptor in prostate cancer cells. *Oncogene* **40**, 4567–4579 (2021).
16. Vélot, L. et al. Proximity-dependent mapping of the androgen receptor identifies Kruppel-like factor 4 as a functional partner. *Mol. Cell. Proteom.* **20**, 100064 (2021).
17. Groner, A. C. et al. TRIM24 is an oncogenic transcriptional activator in prostate cancer. *Cancer Cell* **29**, 846–858 (2016).
18. Le Douarin, B. et al. A possible involvement of TIF1 alpha and TIF1 beta in the epigenetic control of transcription by nuclear receptors. *EMBO J.* **15**, 6701–6715 (1996).
19. Thénot, S., Henriquet, C., Rochefort, H. & Cavaillès, V. Differential interaction of nuclear receptors with the putative human transcriptional coactivator hTIF1. *J. Biol. Chem.* **272**, 12062–12068 (1997).
20. McAvera, R. M. & Crawford, L. J. TIF1 proteins in genome stability and cancer. *Cancers* **12**, 2094 (2020).
21. Herquel, B., Ouararhni, K. & Davidson, I. The TIF1α-related TRIM cofactors couple chromatin modifications to transcriptional regulation, signaling and tumor suppression. *Transcription* **2**, 231–236 (2011).
22. Iyengar, S. & Farnham, P. J. KAP1 protein: an enigmatic master regulator of the genome. *J. Biol. Chem.* **286**, 26267–26276 (2011).
23. Pauletto, E., Eickhoff, N., Padrão, N., Blattner, C. & Zwart, W. TRIMming down hormone-driven cancers: the biological impact of TRIM proteins on tumor development, progression and prognostication. *Cells* **10**, 1517 (2021).
24. Wang, Z. & Patel, D. J. Combinatorial readout of dual histone modifications by paired chromatin-associated modules. *J. Biol. Chem.* **286**, 18363–18368 (2011).
25. Sengupta, B. et al. The effects of histone H2B ubiquitylations on the nucleosome structure and internucleosomal interactions. *Biochemistry* **61**, 2198–2205 (2022).
26. Chen, M. et al. TRIM33 drives prostate tumor growth by stabilizing androgen receptor from Skp2-mediated degradation. *EMBO Rep.* **23**, e53468 (2022).
27. Xiao, L. et al. Targeting SWI/SNF ATPases in enhancer-addicted prostate cancer. *Nature* **601**, 434–439 (2022).
28. Metzger, E. et al. LSD1 demethylates repressive histone marks to promote androgen-receptor-dependent transcription. *Nature* **437**, 436–439 (2005).
29. Fong, K., Zhao, J. C., Song, B., Zheng, B. & Yu, J. TRIM28 protects TRIM24 from SPOP-mediated degradation and promotes prostate cancer progression. *Nat. Commun.* **9**, 5007 (2018).
30. Teng, M., Zhou, S., Cai, C., Lupien, M. & He, H. H. Pioneer of prostate cancer: past, present and the future of FOXA1. *Protein Cell* **12**, 29–38 (2021).
31. Pomerantz, M. M. et al. The androgen receptor cistrome is extensively reprogrammed in human prostate tumorigenesis. *Nat. Genet.* **47**, 1346–1351 (2015).
32. Tan, P. Y. et al. Integration of regulatory networks by NKX3-1 promotes androgen-dependent prostate cancer survival. *Mol. Cell. Biol.* **32**, 399–414 (2012).
33. Luo, M. et al. H3K18ac primes mesendodermal differentiation upon nodal signaling. *Stem Cell Rep.* **13**, 642–656 (2019).
34. Sekirnik, A. R. et al. Identification of histone peptide binding specificity and small-molecule ligands for the TRIM33α and TRIM33β bromodomains. *ACS Chem. Biol.* **17**, 2753–2768 (2022).
35. Xi, Q. et al. A poised chromatin platform for TGF-β access to master regulators. *Cell* **147**, 1511–1524 (2011).
36. Stelloo, S. et al. Endogenous androgen receptor proteomic profiling reveals genomic subcomplex involved in prostate tumorigenesis. *Oncogene* **37**, 313–322 (2018).
37. Nicetto, D. & Zaret, K. S. Role of H3K9me3 heterochromatin in cell identity establishment and maintenance. *Curr. Opin. Genet. Dev.* **55**, 1–10 (2019).
38. Fujimoto, M. et al. HSF1 phosphorylation establishes an active chromatin state via the TRRAP–TIP60 complex and promotes tumorigenesis. *Nat. Commun.* **13**, 4355 (2022).
39. Herquel, B. et al. Transcription cofactors TRIM24, TRIM28, and TRIM33 associate to form regulatory complexes that suppress murine hepatocellular carcinoma. *Proc. Natl. Acad. Sci. USA* **108**, 8212–8217 (2011).
40. Layer, R. M. et al. GIGGLE: a search engine for large-scale integrated genome analysis. *Nat. Methods* **15**, 123–126 (2018).
41. Vickman, R. E. et al. The role of the androgen receptor in prostate development and benign prostatic hyperplasia: a review. *Asian J. Urol.* **7**, 191–202 (2020).
42. Tsherniak, A. et al. Defining a cancer dependency map. *Cell* **170**, 564–576.e16 (2017).
43. Yu, T. et al. Modulation of M2 macrophage polarization by the crosstalk between Stat6 and Trim24. *Nat. Commun.* **10**, 4353 (2019).
44. Zhu, Q. et al. TRIM24 facilitates antiviral immunity through mediating K63-linked TRAF3 ubiquitination. *J. Exp. Med.* **217**, e20192083 (2020).
45. Ali, H. et al. Cellular TRIM33 restrains HIV-1 infection by targeting viral integrase for proteasomal degradation. *Nat. Commun.* **10**, 926 (2019).
46. Han, M. & Sun, Y. Pharmacological targeting of Tripartite Motif Containing 24 for the treatment of glioblastoma. *J. Transl. Med.* **19**, 505 (2021).
47. Bouvier, C. et al. Role of TRIM24 in the regulation of proteasome-autophagy crosstalk in bortezomib-resistant mantle cell lymphoma. *Cell Death Discov.* **11**, 108 (2025).
48. Tsai, W.-W. et al. TRIM24 links a non-canonical histone signature to breast cancer. *Nature* **468**, 927–932 (2010).
49. Linder, S. et al. Drug-induced epigenomic plasticity reprograms circadian rhythm regulation to drive prostate cancer toward androgen independence. *Cancer Discov.* **12**, 2074–2097 (2022).
50. Berger, R. et al. Androgen-induced differentiation and tumorigenicity of human prostate epithelial cells. *Cancer Res.* **64**, 8867–8875 (2004).
51. Stelloo, S. et al. Integrative epigenetic taxonomy of primary prostate cancer. *Nat. Commun.* **9**, 4900 (2018).

52. Mongan, N. P., Tadokoro-Cuccaro, R., Bunch, T. & Hughes, I. A. Androgen insensitivity syndrome. *Best. Pract. Res. Clin. Endocrinol. Metab.* **29**, 569–580 (2015).
53. Fan, W. et al. Androgen receptor null male mice develop late-onset obesity caused by decreased energy expenditure and lipolytic activity but show normal insulin sensitivity with high adiponectin secretion. *Diabetes* **54**, 1000–1008 (2005).
54. Grossmann, M. Low testosterone in men with type 2 diabetes: significance and treatment. *J. Clin. Endocrinol. Metab.* **96**, 2341–2353 (2011).
55. Sato, T. et al. Brain masculinization requires androgen receptor function. *Proc. Natl. Acad. Sci. USA* **101**, 1673–1678 (2004).
56. Akizuki, Y., Kaypee, S., Ohtake, F. & Ikeda, F. The emerging roles of non-canonical ubiquitination in proteostasis and beyond. *J. Cell Biol.* **223**, e202311171 (2024).
57. Severson et al. Epigenetic and transcriptional analysis reveals a core transcriptional program conserved in clonal prostate cancer metastases. *Mol. Oncol.* **15**, 1942–1955 (2021).
58. MacKenzie, T. M. G., Cisneros, R., Maynard, R. D. & Snyder, M. P. Reverse-ChIP techniques for identifying locus-specific proteomes: a key tool in unlocking the cancer regulome. *Cells* **12**, 1860 (2023).
59. Sanjana, N. E., Shalem, O. & Zhang, F. Improved vectors and genome-wide libraries for CRISPR screening. *Nat. Methods* **11**, 783–784 (2014).
60. Jersie-Christensen, R. R., Sultan, A. & Olsen, J. V. Simple and reproducible sample preparation for single-shot phosphoproteomics with high sensitivity. *Methods Mol. Biol.* **1355**, 251–260 (2016).
61. Demichev, V., Messner, C. B., Vernardis, S. I., Lilley, K. S. & Ralser, M. DIA-NN: neural networks and interference correction enable deep proteome coverage in high throughput. *Nat. Methods* **17**, 41–44 (2020).
62. Tyanova, S. et al. The Perseus computational platform for comprehensive analysis of (prote)omics data. *Nat. Methods* **13**, 731–740 (2016).
63. Cox, J. et al. Accurate proteome-wide label-free quantification by delayed normalization and maximal peptide ratio extraction, termed MaxLFQ. *Mol. Cell Proteom.* **13**, 2513–2526 (2014).
64. Stekhoven, D. J. & Bühlmann, P. MissForest—non-parametric missing value imputation for mixed-type data. *Bioinformatics* **28**, 112–118 (2012).
65. Elizarraras, J. M. et al. WebGestalt 2024: faster gene set analysis and new support for metabolomics and multi-omics. *Nucleic Acids Res.* **52**, W415–W421 (2024).
66. Singh, A. A. et al. Optimized ChIP-seq method facilitates transcription factor profiling in human tumors. *Life Sci. Alliance* **2**, e201800115 (2019).
67. Zwart, W. et al. A carrier-assisted ChIP-seq method for estrogen receptor-chromatin interactions from breast cancer core needle biopsy samples. *BMC Genomics* **14**, 232 (2013).
68. Vasimuddin, M., Misra, S., Li, H. & Aluru, S. Efficient architecture-aware acceleration of BWA-MEM for multicore systems. In *2019 IEEE International Parallel and Distributed Processing Symposium (IPDPS)* 314–324 (IEEE, 2019).
69. Ross-Innes, C. S. et al. Differential oestrogen receptor binding is associated with clinical outcome in breast cancer. *Nature* **481**, 389–393 (2012).
70. Ramírez, F. et al. deepTools2: a next generation web server for deep-sequencing data analysis. *Nucleic Acids Res.* **44**, W160–W165 (2016).
71. Yu, G., Wang, L.-G. & He, Q.-Y. ChIPseeker: an R/Bioconductor package for ChIP peak annotation, comparison and visualization. *Bioinformatics* **31**, 2382–2383 (2015).
72. Xu, S. et al. Using clusterProfiler to characterize multiomics data. *Nat. Protoc*. https://doi.org/10.1038/s41596-024-01020-z (2024).
73. Gregoricchio, S. et al. HDAC1 and PRC2 mediate combinatorial control in SPI1/PU.1-dependent gene repression in murine erythroleukaemia. *Nucleic Acids Res.* **50**, 7938–7958 (2022).
74. Bailey, T. L., Johnson, J., Grant, C. E. & Noble, W. S. The MEME Suite. *Nucleic Acids Res.* **43**, W39–W49 (2015).
75. McLeay, R. C. & Bailey, T. L. Motif enrichment analysis: a unified framework and an evaluation on ChIP data. *BMC Bioinforma.* **11**, 165 (2010).
76. Vorontsov, I. E. et al. HOCOMOCO in 2024: a rebuild of the curated collection of binding models for human and mouse transcription factors. *Nucleic Acids Res.* **52**, D154–D163 (2024).
77. Kim, D. et al. TopHat2: accurate alignment of transcriptomes in the presence of insertions, deletions and gene fusions. *Genome Biol.* **14**, R36 (2013).
78. Love, M. I., Huber, W. & Anders, S. Moderated estimation of fold change and dispersion for RNA-seq data with DESeq2. *Genome Biol.* **15**, 550 (2014).
79. Kolde, R. pheatmap: Pretty Heatmaps. 1.0.12 (2010).
80. Li, S. et al. Cistrome-GO: a web server for functional enrichment analysis of transcription factor ChIP-seq peaks. *Nucleic Acids Res.* **47**, W206–W211 (2019).
81. Perez-Riverol, Y. et al. The PRIDE database resources in 2022: a hub for mass spectrometry-based proteomics evidences. *Nucleic Acids Res.* **50**, D543–D552 (2022).

Acknowledgements

We thank the Zwart and Bergman group and the members of the TRIM-Net for discussion and input. The authors would like to thank the Research High Performance Computing (RHPC) facility of the NKI for the infrastructure to analyze the genomics datasets and the Genomics Core Facility (GCF) at the NKI for performing sequencing experiments. W.Z. is supported by the Oncode Institute.

Author contributions

N.E. and W.Z. designed the study and planned experiments. N.E. performed the experiments together with J.J. (non LNCaP knockout data and LNCaP knockout ChIP-seq experiments), S.L. (AR RIME experiments) and N.P. (Antibody validations). Data were analyzed by N.E. with the help of S.G. and J.S. L.H. and O.B. helped planning mass-spec experiments and ran the samples and provided initial data tables. A.B. and W.Z. supervised the experiments and analyses. N.E. and W.Z. wrote the manuscript with input from all authors.

Competing interests

The authors declare no competing interests.

Additional information

Supplementary information The online version contains supplementary material available at https://doi.org/10.1038/s42003-025-08449-2.

Correspondence and requests for materials should be addressed to Andries M. Bergman or Wilbert Zwart.

Peer review information *Communications Biology* thanks Iain (J.) McEwan and the other, anonymous, reviewers for their contribution to the peer review of this work. Primary Handling Editors: Aylin Bircan and Laura Rodriguez Perez. A peer review file is available.